14th Australasian Fluid Mechanics Conference
Adelaide University, Adelaide, Australia
10-14 December 2001

Multi-Fluid Multi-Dimensional Numerical and Experimental Investigation of Dispersed Two-Phase Flow with Wall Liquid Film in the Vicinity of Obstacles

Zoran V. Stosic[1□], Vladimir D. Stevanovic[✧1□] and Akimi Serizawa[2]

[1]Framatome ANP GmbH, Bunsenstr. 43, D-91058 Erlangen, Germany
[2]Department of Nuclear Engineering, Kyoto University, Yoshida, Sakyo, Kyoto, 606-8501, Japan

Abstract

Annular two-phase flow around an obstacle in a vicinity of the channel wall is numerically and experimentally investigated. Numerical simulations of gas phase, entrained droplets and wall liquid film flows were performed with the three-fluid model and with the application of the high order numerical scheme for the liquid film surface interface tracking. Predicted are a separation of gas and entrained droplets streams around the obstacle, as well as a change of wall liquid film thickness in the vicinity of obstacle. Results on liquid film dynamic behaviour are compared with the recently obtained experimental results [4]. Multi-dimensional characteristics of surface waves on the liquid film were measured with newly developed ultrasonic transmission technique in a 3x3 rod bundle test section with air-water flow under atmospheric conditions. Obtained numerical results are in agreement with experimental observations. Presented investigation gives insight into the complex mechanisms of separated two-phase flow with wall liquid film around the obstacle. The obtained results are a support to thermal-hydraulic design and safety analyses of various thermal equipments.

Introduction

Obstacles of various geometries are encountered in the flow channels of thermal equipment. They are a necessary part which support a heat transfer surface mechanical structure, as in the case of spacers in the nuclear reactor fuel rod bundles, or they are introduced in order to enhance heat transfer rates, such as ribs or fins on heat exchangers' surfaces. Obstacles lead to a development of a complex fluid flow structure around them, with enhancement of heat transfer rates and increase of critical heat fluxes (CHFs) as positive effects, and with a hydraulic resistance increase as a drawback. A fluid flow structure around an obstacle is especially complex in the case of the gas-liquid two-phase coolant flow. Depending on the gas phase volume fraction in the two-phase flow stream, an obstacle can lead to various kinds of phase separation and formation of recirculating zones. Recently, a few experimental and numerical investigations were undertaken in order to get insight into the dispersed gas-liquid droplets separation around the obstacle and the wall liquid film behaviour in the vicinity of obstacle. A two-phase flow around rod spacers was experimentally investigated in a 3x3 nuclear fuel rod bundle test section with the air-water flow under atmospheric conditions [4]. Detailed measurements of the liquid film surface structures on the rods were possible with a newly developed ultrasonic transmission technique with a highly rotating reflector. It was shown that the time averaged mean film thickness decreases significantly in the spacer region, with a subsequent recovery downstream from the spacer. The amplitude of large film waves is roughly four times larger than the base film thickness. The same experimental conditions of separated two-phase flow around the spacer were numerically predicted with the application of the MARS method for the liquid film surface tracking [4]. Liquid film, air and droplets flow were simulated in two dimensions with the inclusion of droplets entrainment. A qualitative agreement of numerical and measured results was obtained, but with some quantitative discrepancies. The calculated liquid film velocity is up to 10 times higher than the estimated experimental value, and calculated liquid film thickness downstream from the spacer does not recover to the thickness upstream from the spacer. A numerical study of high-pressure steam and water annular flow around an obstacle was presented in [1]. Vapour and droplets flows were modelled as two-dimensional, while one-dimensional liquid film flow on the wall was considered. The influence of the obstacle on the liquid film flow was demonstrated. In paper [4] both experimental and numerical results shows that the liquid film thickness decrease occurs along the whole gap between the obstacle and the wall, with the film recovery downstream from the obstacle. In [1] a different liquid film dynamics around the obstacle is shown. A rapid liquid film decrease occurs immediately at the wall-obstacle gap entrance, with film thickness recovery already within the gap. Air stream and liquid film interaction in two-dimensional flow around obstacle was numerically investigated in [11], together with parametric analyses of gas phase and liquid film flow rates influence on the film hydro-dynamics. These results showed that liquid film thickness change around obstacle depends on the gas phase velocity, where the increase of gas velocity suppresses the change of mean liquid film thickness. On the other hand, the liquid film flow rate does not have substantial influence on the liquid film thickness change. The separation of gas-droplets dispersed flows around obstacles with and without a fin mounted on its rear end is investigated numerically in [9, 10], but without the inclusion of the liquid film flow on the wall.

In this paper the numerical investigation of annular two-phase flow around an obstacle in the vicinity of the channel wall is performed. Numerical simulations of gas phase, entrained droplets and wall liquid film flows were performed with the three-fluid model and with the application of a high order numerical scheme for liquid film surface interface tracking. Results of the separation of gas and entrained droplets streams around the obstacle, as well as the change of wall liquid film thickness in the vicinity of obstacle are presented. Predicted liquid film dynamic behaviour is compared with the recently obtained experimental results [4] and a good agreement is shown. Here presented modelling approach is an improvement of the previous works [9, 10, 11] in a sense that the coupled calculation of dispersed two-phase flow separation around the obstacle with the prediction of the liquid film hydro-dynamics on the wall is performed.

Modelling Approach

A two-dimensional, three-fluid model is applied for the numerical simulation of annular two-phase flow around the obstacle. Mass and momentum fluid flow conservation equations are written for gas, entrained droplets and liquid film flow on the wall. Interface transfer processes are modelled by "closure laws".

✧Temporarily at Framatome ANP GmbH, P.O.Box 3220, D-91050 Erlangen, Germany
□A.T.H.A. – Advanced Thermal Hydraulics with Applications. e-Mail: Zoran@Stosic.de , URL: http://www.Stosic.de

Modelling Assumptions and Features

a) Two-dimensional separated air and water two-phase flow is modelled. Liquid film flows on the wall. Air and liquid film streams are continuous, while droplets are dispersed within gas core. The liquid film surface has a finite thickness observed as a dispersed two-phase flow. Starting from the continuous liquid film area, in the direction perpendicular to the main flow direction, figure 1, the water volume fraction changes from 1 to the finite value determined by the amount of droplets dispersed in continuous gas flow. The thickness of the interface is determined with the ability of the applied numerical method to track front propagation. Here applied third order numerical method is able to track interface within two to four control volumes [6].
b) Due to the three-fluid model formulation, the slip between gas-droplets, gas-liquid film and droplets-liquid film is taken into account.
c) Droplet deposition is inherently included into the two-dimensional formulation of the applied three-fluid model. Namely, entrained droplets flow in two-dimensions and deposition takes place when droplets reach the gas-liquid film interface area. At that instant the entrained droplets void fraction is added to the liquid film void fraction. Assumed lower practical value for liquid film interface existence is 0.001.
d) Droplets entrainment from the liquid film surface into the gas core is calculated with a correlation developed for one-dimensional separated two-phase flow [7].
e) The flow is adiabatic under atmospheric conditions. Hence, the energy conservation equations are omitted.
f) The two-phase flow is observed as semi-compressible, that is the acoustic flow effects are neglected, while the influence of the pressure change on the vapour and liquid thermo-physical properties is taken into account. This assumption is valid since the two-phase velocity is not higher than 20 m/s – 30 m/s.
g) Turbulence is modelled with the k-ε model in both phases.
h) The surface tension is taken into account at the liquid film surface as the continuous body force determined by the liquid volume spatial distribution.

Governing Equations

Conservation equations take the following form in the indicial notation.

Continuity equation

$$\frac{\partial \alpha_k \rho_k}{\partial t} + \frac{\partial\left(\alpha_k \rho_k u_{k,i}\right)}{\partial x_i} = m_k''' \tag{1}$$

Momentum conservation

$$\frac{\partial\left(\alpha_k \rho_k u_{k,i}\right)}{\partial t} + \frac{\partial\left(\alpha_k \rho_k u_{k,i} u_{k,j}\right)}{\partial x_j} = -\alpha_k \frac{\partial p}{\partial x_i} + \frac{\partial}{\partial x_j}\left[\alpha_k(\rho_k \eta_k \frac{\partial u_{k,i}}{\partial x_j} - \rho_k \overline{u'_{k,i} u'_{k,j}})\right] + \alpha_k \rho_k g_i + \Sigma F_{k,i} + (\Sigma m''' u)_{k,i} \tag{2}$$

In Eqs. (1,2) index k is 1 for entrained droplets, 2 for gas phase and 3 for liquid film. Parameters α_k, $u_{k,i}$ and p are phase volume fraction, time averaged instantaneous velocity and pressure, respectively. As the consequence of the instantaneous equations time averaging the following turbulent (Reynolds) stress tensor term appears $\overline{u'_{k,i} u'_{k,j}}$. The source terms on the r.h.s. of Eqs. (1)-(2) are as follows.

$$m_1''' = m_e''' - m_d''' \tag{3}$$

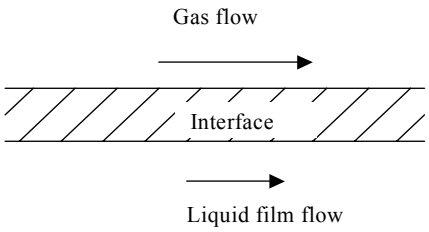

Figure 1. A finite thickness of the modelled liquid film surface

$$m_2''' = 0 \tag{4}$$

$$m_3''' = m_d''' - m_e''' \tag{5}$$

where m_e''' and m_d''' are entrainment and deposition rates per unit volume, respectively. Sums of the interfacial forces per unit volume are

$$\sum \vec{F}_1 = \vec{F}_{21} + \vec{F}_{VM} + \vec{F}_{L1} \tag{6}$$

$$\sum \vec{F}_2 = -\vec{F}_{21} - \vec{F}_{23} - \vec{F}_{VM} - \vec{F}_{L1} - \vec{F}_\sigma \tag{7}$$

$$\sum \vec{F}_3 = \vec{F}_{23} + \vec{F}_\sigma \tag{8}$$

where $\vec{F}_{21}$ and $\vec{F}_{31}$ are gas-droplets and gas-liquid film interfacial forces respectively, $\vec{F}_{VM}$ is virtual mass force, $\vec{F}_{L1}$ is lateral force and $\vec{F}_\sigma$ is surface tension force. Interfacial forces caused by momentum transfer due to droplets entrainment and deposition are given by

$$(\sum m''' u)_{1,i} = m_e''' u_{3,i} - m_d''' u_{1,i} \tag{9}$$

$$(\sum m''' u)_{2,i} = 0 \tag{10}$$

$$(\sum m''' u)_{3,i} = -m_e''' u_{3,i} + m_d''' u_{1,i} \tag{11}$$

Volume fraction balance equation is also included

$$\alpha_1 + \alpha_2 + \alpha_3 = 1 \tag{12}$$

Turbulence Modelling

The Boussinesq's eddy viscosity concept is applied, which is generalized in the following form for momentum turbulent transport

$$-\overline{u'_{k,i} u'_{k,j}} = \eta_{k,t}\left(\frac{\partial u_{k,i}}{\partial x_j} + \frac{\partial u_{k,j}}{\partial x_i}\right) - \frac{2}{3} k_k \delta_{ij} \tag{13}$$

The Kolmogorov-Prandtl relation is applied for the eddy viscosity prediction

$$\eta_{k,t} = c_\mu \frac{k_k^2}{\varepsilon_k} \tag{14}$$

Turbulent kinetic energy and dissipation are predicted by the two-equation k-ε model, which has the following form in Cartesian coordinate system

Turbulence Kinetic Energy Equation

$$\frac{\partial\left(\alpha_k \rho_k k_k\right)}{\partial t} + \frac{\partial\left(\alpha_k \rho_k u_{k,i} k_k\right)}{\partial x_i} = \frac{\partial}{\partial x_i}\left(\alpha_k \Gamma_{k,k} \frac{\partial k_k}{\partial x_i}\right) + \alpha_k (P_k - \rho_k \varepsilon_k) \tag{15}$$

Turbulence Dissipation Rate Equation

$$\frac{\partial\left(\alpha_k\rho_k\varepsilon_k\right)}{\partial t}+\frac{\partial\left(\alpha_k\rho_k u_{k,i}\varepsilon_k\right)}{\partial x_i}= \frac{\partial}{\partial x_i}\left(\alpha_k\Gamma_{k,\varepsilon}\frac{\partial\varepsilon_k}{\partial x_i}\right)+\alpha_k C_{\varepsilon 1}P\frac{\varepsilon}{k}-\alpha_k C_{\varepsilon 2}\rho\frac{\varepsilon^2}{k} \quad (16)$$

where P_k is the turbulent kinetic energy production for the phase k

$$P_k=\rho_k\eta_{k,t}\left[\left(\frac{\partial u_{k,i}}{\partial x_j}\right)+\left(\frac{\partial u_{k,j}}{\partial x_i}\right)\right]\left(\frac{\partial u_{k,i}}{\partial x_j}\right) \quad (17)$$

and diffusion coefficients are given by

$$\Gamma_{k,k}=\rho_k\left(\eta_k+\frac{\eta_{k,t}}{\sigma_k}\right) \quad (18)$$

and

$$\Gamma_{k,\varepsilon}=\rho_k\left(\eta_k+\frac{\eta_{k,t}}{\sigma_\varepsilon}\right) \quad (19)$$

Empirical constants are presented in the following Table.

Table 1 Empirical constants for the standard k-ε model

c_μ	$C_{\varepsilon 1}$	$C_{\varepsilon 2}$	σ_k	σ_ε
0.09	1.44	1.92	1.0	1.3

Boundary turbulent flow parameters are predicted with the "wall functions" at the flow channel wall and spacer's surface.

Closure Laws

The interfacial drag force is calculated as

$$F_{21,i}=\frac{3}{4}\alpha_2\rho_1\frac{C_D}{D_p}\sqrt{\sum_{j=1}^{3}(u_{2,j}-u_{1,j})^2}\,(u_{2,i}-u_{1,i}) \quad (20)$$

where C_D is the interfacial drag coefficient, and D_p is the diameter of the dispersed particle. For dispersed flow patterns, C_D is proportional to the square of the vapour velocity [8]

$$C_D=0.15D_p\left(\frac{g\Delta\rho}{\sigma}\right)^{1/2}\left(1-\alpha_2\right)\mu_2^2 \quad (21)$$

The surface tension force is calculated as

$$F_{\sigma,i}=\sigma(\delta_{ji}-n_j\cdot n_i)\left|\nabla\alpha\right| \quad (22)$$

where

$$\vec{n}=\frac{\nabla\alpha}{\left|\nabla\alpha\right|} \quad (23)$$

The lift force acts on the droplets in the direction perpendicular to the relative velocity [3]

$$F_{L2,i}=C_L\rho_2\alpha_1\left[(u_{2,j}-u_{1,j})\frac{\partial u_{2,j}}{\partial x_i}-(u_{2,j}-u_{1,j})\frac{\partial u_{2,i}}{\partial x_j}\right] \quad (24)$$

Here the adopted value for C_L=0.1 is similar to the value used for bubbly dispersed flow.

The virtual mass force arises in the transient flow due to the force required to accelerate the apparent mass of surrounding phase when the relative velocity changes. It is given with [2]

$$F_{VM,i}=C_{VM}\alpha_2\rho_1\left(\frac{\partial u_{2,i}}{\partial t}+u_{2,j}\frac{\partial u_{2,i}}{\partial x_j}-\frac{\partial u_{1,i}}{\partial t}-u_{1,j}\frac{\partial u_{1,i}}{\partial x_j}\right) \quad (25)$$

where the values for C_{VM} are determined as in case of bubbly two-phase flow in the range $1.2<C_{VM}<3.4$.

Droplets entrainment from the liquid film surface is calculated according to [7] with

$$m_e''=1.1\cdot 10^4\,\delta^{2.25}\rho_1 \quad (26)$$

where m_e'' is the mass of entrained droplets per unit film surface and unit time in (kg/m^{2}s). The entrainment mass rate in Eqs. (3) and (5) should be calculated per unit volume, m_e''' in (kg/m^{3}s). Assuming that the liquid film surface is mainly parallel to the horizontal x-axis, the volumetric rate of droplets entrainment m_e''' is obtained from Eq. (26) by dividing it with Δy - the height of the control volume which comprises liquid film surface.

Numerical Experiments Boundary Conditions

The flow channel geometry and applied numerical mesh are shown in Fig. 2. The obstacle is positioned in the narrow channel, 1 mm from the wall. The obstacle length is 30 mm and width is 0.5 mm. These dimensions correspond to the geometry of one flow channel in the 3x3 rod bundle experimental test section [4]. A chosen channel length is sufficient to comprise the relaxation length downstream the spacer. Dimensions of the control volume are 2x0.05 mm and the flow domain is discretized with 50x40 control volumes in x and y direction respectively. Further refinement of the computational mesh has shown no practical change in predicted velocity fields and film thickness. This insensitivity to the grid refinement is attributed to the approximately parabolic nature of the flow, where the fluid streams are directed along the flow channel length. Except the steam and droplets impingement at the obstacle front end and the transition from the obstacle-wall gap to the obstacle downstream area, the fluid streams are upstream dominated with negligible influence of the downstream flow conditions. Axis of symmetry is assumed at the channel upper boundary with the so called "adiabatic" conditions for all flow parameters. Zero change of the flow parameters is taken at the channel exit. Uniform inlet air (18 m/s), droplets (14 m/s) and liquid film (0.5 m/s) velocity profiles are adopted. No velocity slip conditions are applied at the channel walls and at the obstacle surface. "Wall functions" are used for the prediction of turbulent kinetic energy and dissipation rate at the channel wall and obstacle surface.

Numerical Method of Solution

The control volume based finite difference method is applied for the numerical solution of momentum conservation equations and a newly developed third order accurate numerical scheme for the solution of the liquid phase volume fraction conservation (propagation) equation [6]. A pressure-correction equation is derived according to the SIMPLE numerical method [5] from the momentum and mass balance equations.

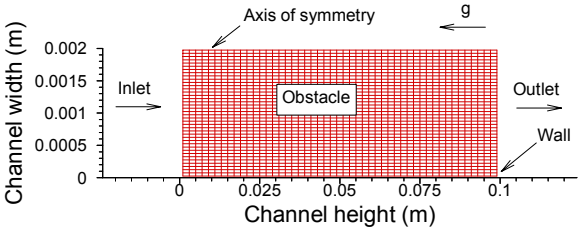

Figure 2. Geometry of the flow channel and numerical mesh

Two-dimensional flow field is discretized with rectangular control volumes. Two grids are formed, the basic one for the solution of scalar parameter equations (void fraction conservation equation and pressure correction equation) and a staggered grid for the solution of the momentum equations (prediction of velocity fields). The convection terms in momentum equations are approximated with upwind finite differences, while diffusion and source terms are approximated with central differences. Fully implicit time integration is applied. The resulting set of discretized momentum equations is solved iteratively by the Alternating Direction Implicit (ADI) method. For the calculation of a steady-state condition, the transient calculation procedure is performed with constant boundary conditions.

A third order accurate numerical method is applied to the solution of gas-liquid interface tracking in two-phase flow [6]. The method is based on the transformation of the liquid volume fraction conservation equation into the form with the substantial derivative and the approximation of the substantial derivative with the finite difference along the fluid particle characteristic path. The fluid particle characteristic path in the temporal-spatial system is tracked from the solution of the momentum conservation equation. The initial value of the scalar parameter on the characteristic path is predicted by the application of the Lagrange interpolation polynomial of the third degree in two-dimensional space. The method effectively suppresses numerical diffusion and enables the interface tracking in two-phase flow by the application of the standard two-fluid model.

Results and Discussions

Figure 3 shows numerical results of the air-droplets separation around obstacle and the liquid film thickness change on the wall. Droplets impact at the front edge of the obstacle and a stream of droplets is directed from the edge towards the wall liquid film. These droplets are deposited at the film, leading to an increase of the film thickness. A liquid film thinning is calculated in the gap between the wall and obstacle, with the subsequent increase of the film thickness downstream from the obstacle. The liquid film thickness decrease is caused by the air stream acceleration and liquid film-air interfacial shear stress increase in the gap, while downstream film thickness recovery is caused by the air de-acceleration and deposition of droplets, which separate from the air stream in the dispersed flow around the obstacle. The liquid film thinning around the obstacle and subsequent downstream film thickness increase are experimentally observed [4]. Also, large amplitude film waves with film bridging from the wall to the obstacle are experimentally observed. Numerical results indicate that the liquid film bridging is triggered within the intensive droplets current from the obstacle front edge to the liquid film. Air velocity profiles are shown in figure 4. Airflow acceleration in the wall-obstacle gap is clearly presented. Also, it is shown that the position of the air velocity vectors close to the wall change according to the change of the liquid film thickness. Comparing figures 4 and 5 it is seen that droplets and air velocity fields are similar.

Conclusions

Two-dimensional numerical investigation of annular two-phase flow around the flow channel obstacle is performed. Coupled liquid droplets and wall liquid film flow behaviour is shown. Strong droplet separation from the air stream at the obstacle front edge is obtained with the subsequent deposition on the wall film. Predicted liquid film thinning in the wall-obstacle gap is in agreement with experimental evidence.

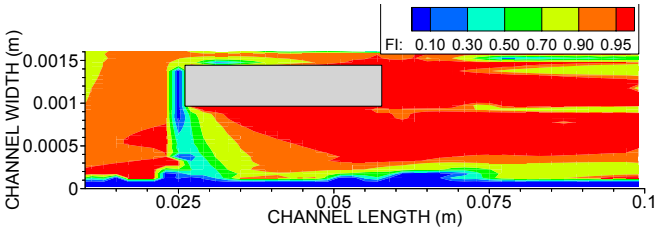

Figure 3. Air void fraction distribution around the obstacle

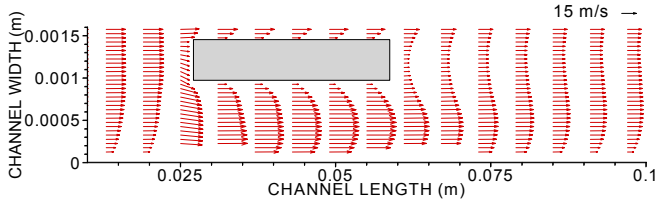

Figure 4. Air velocity profiles

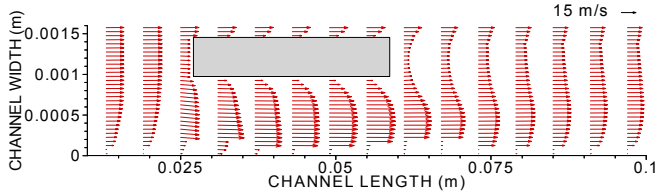

Figure 5. Water velocity profiles

References

[1] Antal, S. P., Nagrath, S. & Podowski, M. Z., Multidimensional Simulations of Two-Phase Flows in Large Volumes with Injection Spargers, *4th Int. Conference on Multiphase Flow*, New Orleans, USA, May 27-June 1, 2001.

[2] Ishii, M., Two-fluid Model for Two-phase Flow, *2nd International Workshop on Two-Phase Flow Fundamentals*, Rensselaer Polytechnic Institute, USA, 1987.

[3] Lahey, R. T., The Analysis of Phase Separation and Phase Distribution Phenomena using Two-Fluid Models, *3rd Int. Topical Meeting on Nuclear Power Plant Thermal-Hydraulics and Operation*, Seul, Korea, November, 1988, A1-69-87.

[4] Noriyasu, K., Kumagai, K., Tsuji, Y., Kunugi, T. & Serizawa, A., Multi-dimensional Characteristics of Surface Waves on the Liquid Film Flow in a 3x3 Rod Bundle, *4th Int. Conference on Multiphase Flow*, New Orleans, USA, May 27-June 1, 2001.

[5] Patankar, S., *Numerical Heat Transfer and Fluid Flow*, Hemisphere Publ. Co., 1980.

[6] Stevanovic, V., High-Order Accurate Scheme for the Numerical Solution of Scalar Parameter Transport Equation Applied to Enthalpy Transport and Interface Tracking, *4th Int. Conference on Multiphase Flow*, New Orleans, Louisiana, USA, May 27-June 1, 2001.

[7] Stevanovic, V., et al., A Simple Model for Vertical Annular and Horizontal Stratified Two-Phase Flows with Liquid Entrainment and Phase Transitions: One-Dimensional Steady State Conditions, *Nuclear Engineering and Design*, **154**, 1995, 357-379.

[8] Stosic, Z. & Stevanovic, V., A Numerical Approach to the Simulation of One-Phase and Two-Phase Reactor Coolant Flow around Nuclear Fuel Spacers, *9th Int. Conference on Nuclear Engineering - ICONE 9*, Nice, France, April 8-12, 2001.

[9] Stosic, Z. & Stevanovic, V., Prediction of Thermal and Hydraulic Relaxation Length Behind Obstacle in Two-Phase Turbulent Coolant Flow, *39th European Two-Phase Flow Group Meeting*, Aveiro, Portugal, June 17-20, 2001.

[10] Stosic, Z. & Stevanovic, V., The influence of spacer's fin angle on two-phase flow separation, *2nd Int. Conference on Computational Heat and Mass Transfer COPPE/EE/UFRJ,* Federal University of Rio de Janeiro, Brazil, October 22-26, 2001.

[11] Stosic, Z., Stevanovic, V. & Serizawa, A., Two-phase flow separation in the vicinity of obstacle: liquid film flow hydro-dynamics, *1st Int. Conference on Heat Transfer, Fluid Mechanics and Thermodynamics*, Kruger Park, South Africa, April 8-10, 2002.